Journal of Biomolecular NMR, **20:** 275–285, 2001.
KLUWER/ESCOM

The use of TROSY for detection and suppression of conformational exchange NMR line broadening in biological macromolecules

Konstantin Pervushin
Laboratorium für Physikalische Chemie, Eidgenössische Technische Hochschule, CH-8092 Zürich, Switzerland

Received 18 January 2001; Accepted 10 May 2001

Key words: conformational exchange, cross-correlation, spin relaxation, TROSY

Abstract

The interference between conformational exchange-induced time-dependent variations of chemical shifts in a pair of scalar coupled ^{1}H and ^{15}N spins is used to construct novel TROSY-type NMR experiments to suppress NMR signal loss in [^{15}N,^{1}H]-correlation spectra of a 14-mer DNA duplex free in solution and complexed with the *Antp* homeodomain. An analysis of double- and zero-quantum relaxation rates of base ^{1}H–^{15}N moieties showed that for certain residues the contribution of conformational exchange-induced transverse relaxation might represent a dominant relaxation mechanism, which, in turn, can be effectively suppressed by TROSY. The use of the new TROSY method for exchange-induced transverse relaxation optimization is illustrated with two new experiments, 2D $^{h1}J_{HN}$,$^{h2}J_{NN}$-quantitative [^{15}N,^{1}H]-TROSY to measure $^{h1}J_{HN}$ and $^{h2}J_{NN}$ scalar coupling constants across hydrogen bonds in nucleic acids, and 2D ($^{h2}J_{NN} + {}^{h1}J_{NH}$)-correlation-[^{15}N,^{1}H]-TROSY to correlate $^{1}H^{N}$ chemical shifts of bases with the chemical shifts of the tertiary ^{15}N spins across hydrogen bonds using the sum of the trans-hydrogen bond coupling constants in nucleic acids.

Abbreviations: TROSY, transverse relaxation-optimized spectroscopy; DD, dipole–dipole coupling; CSA, chemical shift anisotropy; CSX, conformational exchange-induced relaxation; 2D, two-dimensional; DSS, 2,2-dimethyl-2-silapentane-5-sulfonate sodium salt.

Introduction

The TROSY principle (Pervushin et al., 1997) is usually referred to the use of the interference between dipole–dipole coupling (DD) and chemical shift anisotropy (CSA) (Shimizy, 1964; Goldman, 1984) or between two remote CSA interactions (Kumar and Kumar, 1996) to suppress or at least reduce transverse relaxation in two heteronuclear spin systems such as ^{1}H–^{13}C and ^{1}H–^{15}N moieties in proteins and nucleic acids (Pervushin et al., 1997, 1998b, 1999; Brutscher et al., 1998; Meissner and Sorensen, 1999; Yang and Kay, 1999). Since then, new TROSY-type experiments have been proposed which rely on the DD/CSA interference in ^{13}C–^{13}C spin systems (Riek et al., 2000) or the interference between nuclear spin DD and CSA interactions and the electron Curie spin in paramagnetic proteins (Boisbouvier et al., 1999; Madhu et al., 2000). Those interactions are modulated by rotational molecular motions of biomolecules and thus impose a dominant impact on the size limit for biomacromolecular structures that can be studied by NMR spectroscopy in solution (Wider and Wüthrich, 1999).

A dynamic exchange between different conformational or chemical states with the characteristic time scale of microseconds to milliseconds frequently represents yet another significant transverse relaxation mechanism in biomolecules (Kaplan and Fraenkel, 1980; Sandstrom, 1982). Typical examples of biomolecular conformational exchange include a ligand exchanging between free and receptor-bound forms (Moseley et al., 1997), proteins in equilibrium between native and denatured forms (Neri et al., 1992; Farrow et al., 1994), proteins exhibiting local conformational dynamics in backbone or side chains

(Szyperski et al., 1993; Nicholson et al., 1995), and DNA duplexes existing in an equilibrium between two or more distinct conformations (Feigon et al., 1983, 1984; Choe et al., 1991; Fernandez et al., 1998; Pervushin et al., 2000).

The presence of the slow motional processes which cause a modulation of the isotropic chemical shifts of two nuclei involved in multiple-quantum coherences can be manifested in significantly different relaxation of the zero- and double-quantum coherences (Rance, 1988; Kloiber and Konrat, 2000; Tessari and Vuister, 2000). Here we propose the use of the differential conformational exchange-induced transverse relaxation (CSX) in the ZQ and DQ coherences to optimize transverse relaxation properties of the heteronuclear spin coherences evolving in multinuclear NMR experiments. It should be noted, however, that the intermolecular chemical exchange processes, such as the exchange of the labile protons with solvent water usually result in the decorrelation of the involved two-spin coherences (Skrynnikov and Ernst, 1999), the process which cannot be reversed by TROSY-type approaches. The use of the new TROSY method for the conformational exchange-induced transverse relaxation optimization is illustrated by two new experiments, 2D $^{h1}J_{HN}$,$^{h2}J_{NN}$-quantitative [^{15}N,^{1}H]-TROSY to measure $^{h1}J_{HN}$ and $^{h2}J_{NN}$ scalar coupling constants across hydrogen bonds in nucleic acids, and 2D ($^{h2}J_{NN}$+ $^{h1}J_{NH}$)-correlation-[^{15}N,^{1}H]-TROSY to correlate ^{1}H^{N} chemical shifts of bases with the chemical shifts of the tertiary ^{15}N spins across hydrogen bonds using the sum of the trans-hydrogen bond coupling constants.

Theory

We consider a molecule which may exchange among several discrete conformations bearing rigidly attached two scalar coupled spins $\frac{1}{2}$, I and S, with a time-independent scalar coupling constant J_{IS}. If the spins have a time dependent chemical shift $\delta\omega(t)$, the spin Hamiltonian in the absence of external rf-fields is:

$$\mathcal{H}(t) = \mathcal{H}_{\rm o} + \mathcal{H}^{\rm DD}(t) + \mathcal{H}^{\rm CSA}(t) + \mathcal{H}^{\rm CSX}(t) \quad (1a)$$

$$\mathcal{H}^{\rm CSX}(t) = \delta\omega_{\rm I}(t) I_{\rm z} + \delta\omega_S(t) S_z \quad (1b)$$

where $\mathcal{H}_{\rm o}$, $\mathcal{H}^{\rm DD}(t)$ and $\mathcal{H}^{\rm CSA}(t)$ are the usual Hamiltonians describing Zeeman, spin-coupling, dipole–dipole and chemical shift anisotropy interactions in the *IS* spin system. For spins exchanging between sites with different chemical shifts, the term $\mathcal{H}^{\rm CSX}(t)$ provides a relaxation mechanism (Deverell et al., 1970) frequently manifested in biomacromolecules as chemical or conformational exchange line broadening (Kaplan and Fraenkel, 1980; Sandstrom, 1982).

The evolution of the zero- and double-quantum manifolds of the *IS* spin system is given by Equation 2, derived by the direct integration of the standard Wangsness–Bloch–Redfield master equation for the density operator (Abragam, 1961):

$$\frac{d}{dt}\begin{bmatrix} \langle I^{\pm}S^{\mp}\rangle \\ \langle I^{\pm}S^{\pm}\rangle \end{bmatrix} = -\begin{bmatrix} \pm i(\omega_{ZQ}) + R_{ZQ} + R_{ZQ}^{csx} & 0 \\ 0 & \pm i(\omega_{DQ}) + R_{DQ} + R_{DQ}^{csx} \end{bmatrix} \cdot \begin{bmatrix} \langle I^{\pm}S^{\mp}\rangle \\ \langle I^{\pm}S^{\pm}\rangle \end{bmatrix} \quad (2)$$

The abbreviations $ZQ_{\pm} = I_{\mp}S_{\pm}$ and $DQ_{\pm} = I_{\pm}S_{\pm}$ are used for the zero-quantum and double-quantum operators, respectively. $\omega_{ZQ} = \omega_I - \omega_S$ and $\omega_{DQ} = \omega_I + \omega_S$ are the difference and sum of the Larmor frequencies of the spins I and S, R_{ZQ} and R_{DQ} are relaxation rates by mechanisms of relaxation due to DD coupling between the spins I and S and CSA of the spins I and S given by Equations 3. In this formulation Equation 3b represents the auto-correlated relaxation rate due to CSA and DD interactions within *IS* spin system and Equation 3c provides the cross-correlated relaxation rate due to the interference between CSA of I and S spins (Pervushin et al., 1999).

$$R_{ZQ,DQ} = R_{auto} \mp R_{cc}^{csa}, \quad (3a)$$

$$R_{auto} = 4(\delta_I^2 + \delta_S^2)J(0) + 3\delta_I^2 J(\omega_I) + 3\delta_S^2 J(\omega_S) + 3p^2(J(\omega_I) + J(\omega_S) + 4J(\omega_I + \omega_S)) \quad (3b)$$

$$R_{cc}^{csa} = 8C_{IS}\delta_I\delta_S J(0) \quad (3c)$$

Signs '−' and '+' correspond to the zero- and double-quantum coherences, respectively, $p = \frac{1}{2\sqrt{2}}\gamma_I\gamma_S\hbar/r_{IS}^3$, $\delta_S = \frac{1}{3\sqrt{2}}\gamma_S B_0 \Delta\sigma_S$ and $\delta_I = \frac{1}{3\sqrt{2}}\gamma_I B_0 \Delta\sigma_I$, where γ_I and γ_S are the gyromagnetic ratios of I and S, $\hbar$ is the Planck constant divided by 2π, r_{IS} the distance between I and S, B_0 the polarizing magnetic field, and $\Delta\sigma_I$ and $\Delta\sigma_S$ are the differences between the axial and the perpendicular principal components of the axially symmetric chemical shift tensors of spins I and S, respectively.

$C_{kl} = 0.5(3\cos^2\Theta_{kl} - 1)$ and Θ_{kl} is the angle between the unique CSA tensor axes of the spins I and S. Functions $J(\omega)$ represent the spectral density at the frequencies indicated:

$$J(\omega) = \frac{2\tau_c}{5(1 + (\tau_c\omega)^2)} \tag{4}$$

where τ_c is the correlation time of isotropic tumbling of the rigid molecule.

Following the standard treatment of the spectral densities for the N-site jump model (Tropp, 1980), the relaxation rates R^{csx} of the zero- and double-quantum manifolds due to chemical or conformational exchange can be related to the products of the probability functions given by Equation 5:

$$\begin{aligned} R_m^{csx} &= \int_0^\infty \langle \delta\omega_m(0) \cdot \delta\omega_m(t) \rangle \, dt \\ &= \int_0^\infty \left(\sum_{i,j=1}^{N} \langle P_i \rangle \, P(j,t|i,0) \delta\omega_m^i \cdot \delta\omega_m^j \right) dt \end{aligned} \tag{5}$$

where $m = ZQ$ or DQ. $\langle P_i \rangle$ is the *a priory* probability to find a molecule in the i-th site with the chemical shifts $\delta\omega_m^i$ and $P(j,t|i,0)$ is the conditional probability to find the molecule in the j-th site with the chemical shifts at a time t, given that it occupied the i-th site at time zero.

For the following discussion of the influence of lattice motion, the explicit introduction of a particular model of the exchange process is required. Since in the current work we focus on the use of the TROSY-type relaxation compensation to suppress exchange line broadening, it is instructive, first, to evaluate the relaxation rates of Equation 5 for a simple two-site lattice jump model and, then, compare them with the results for an N-site exchange process with a large number of exchanging sites. The former situation might be encountered in relatively rigid proteins, nucleic acids or their complexes, while the latter case can be pertinent to unfolded or partially folded proteins where a dynamic equilibrium between many conformational configurations occurs (Mok et al., 1999).

For the two-site jump model with the populations P_1, P_2 and the jump rate $1/(2\tau_{ex}) = \kappa_1 P_1 = \kappa_2 P_2$ the relaxation rates are given by Equations 6:

$$R_{ZQ,DQ}^{csx} = R_{auto}^{csx} \mp R_{cc}^{csx}, \tag{6a}$$

$$R_{auto}^{csx} = 2P_1P_2((\Delta\delta\omega_I^{12})^2 + (\Delta\delta\omega_S^{12})^2)\tau_{ex} \tag{6b}$$

$$R_{cc}^{csx} = 4P_1P_2\Delta\delta\omega_I^{12}\Delta\delta\omega_S^{12}\tau_{ex} \tag{6c}$$

where $\Delta\delta\omega_{I,S}^{ij} = \Delta\delta\omega_{I,S}^{i} - \Delta\delta\omega_{I,S}^{j}$ is the difference in the chemical shifts between sites i and j. Equation 6b represents the auto-correlated CSX relaxation rate and Equation 6c provides the cross-correlated CSX relaxation rate. Note, that for $|\Delta\delta\omega_I^{12}| \cong |\Delta\delta\omega_S^{12}|$, total CSX relaxation of one of the two (zero- or double-quantum) coherences is greatly reduced. The coherence experiencing reduced transverse relaxation is defined by the sign of the frequency change in the route from site 1 to site 2.

Next, we consider exchange between N equally populated sites $P_1 = P_2 = \ldots = P_N = 1/N$ with the rates $\kappa_{ij} = 1/(2\tau_{ex})(1-\delta_{ij})N$, where $i, j = 1..N$. The corresponding relaxation CSX rates can be directly derived from Equation 5, resulting in Equation 7.

$$R_m^{csx} = \frac{1}{N^4} \sum_{i,j=1}^{N} (\Delta\delta\omega_m^{i,j})^2\tau_{ex} + \left(\frac{\delta(\omega)}{N} \sum_{i=1}^{N} \delta\omega_m^i \right)^2 \tag{7}$$

The second sum in Equation 7 represents the averaged chemical shift and $\delta(\omega)$ is the spectral density function of the time independent averaged chemical shift such that $\delta(\omega) = 1$ for $\omega = 0$ and 0 for all other frequencies. This term does not cause relaxation and generally can be included into the coherent part of the hamiltonian, resulting in the CSX relaxation rate given by Equation 8.

$$R_m^{csx} = \frac{1}{N^4} \sum_{i,j=1}^{N} (\Delta\delta\omega_m^{i,j})^2\tau_{ex} \tag{8}$$

Expansion of Equation 8 relative to $\Delta\delta\omega_m^{i,j}$ results in the expression for the CSX relaxation rates of the zero- and double-quantum coherences for the N-site exchange model given by Equation 9:

$$\begin{aligned} R_{ZQ,DQ}^{csx} &= \frac{\tau_{ex}}{N^2} \sum_{i,j=1}^{N} [(\Delta\delta\omega_I^{i,j})^2 + (\Delta\delta\omega_S^{i,j})^2] \\ &\quad \mp \frac{2\tau_{ex}}{N^2} \sum_{i,j=1}^{N} \Delta\delta\omega_I^{i,j}\Delta\delta\omega_S^{i,j} \end{aligned} \tag{9}$$

where the signs '−' and '+' correspond to the zero- and double-quantum coherences, respectively. The first sum in Equation 9 represents the auto-correlated CSX relaxation rate and the second sum is the cross-correlated relaxation. Since the change of the sign and the absolute values of $\Delta\delta\omega_I^{i,j}$ and $\Delta\delta\omega_S^{i,j}$ can be considered to be uncorrelated for large N, the relative contribution of the cross-correlated term to CSX relaxation rapidly decreases with the increase of N.

Thus, for the case of the exchange process between two conformations, the complete cancellation of CSX transverse relaxation can be theoretically achieved provided that variations in the chemical shifts of the I and S spins between two exchanging conformations are comparable. Note that the population factors and the exchange rate do not impose any limitation on the efficiency of the relaxation compensation. In contrast to the TROSY effect utilizing DD/CSA or CSA/CSA interference, either one of the zero- or double-quantum coherences may exhibit preferable relaxation properties, depending on the relative configuration of the two exchanging sites. The rapid deterioration of the relaxation compensation effect is expected if the exchange process proceeds via a large number of exchanging sites.

Materials and methods

The structure of the DNA duplex used for this study corresponds to a minimal fragment of the *BS2* operator site that is recognized by the *Antp* and *fushi tarazu* homeodomains (Muller et al., 1988). The synthesis of the uniformly ^{13}C,^{15}N-labeled duplex, which yields ^{15}N-^{1}H-correlation cross peaks for all but the terminal base pairs, and the partially labeled duplex with isotope labels only on the selected nucleotides, which yields ^{15}N–^{1}H-correlation peaks for G^{5}, G^{12} and T^{21}, were described elsewhere (Fernandez et al., 1998; Pervushin et al., 1998a). In the protein complex the uniformly labeled DNA was bound to a uniformly ^{15}N-labeled 69-residue polypeptide construct containing the *Antp* homeodomain in positions 1–60 (Muller et al., 1988). NMR experiments are performed on a Bruker *Avance* 800 MHz spectrometer.

Basic 2D [^{15}N,^{1}H]-zero- and double-quantum TROSY experiment

To observe differential ZQ/DQ relaxation we introduce a 2D [^{15}N,^{1}H]-zero-quantum-double-quantum-TROSY experiment (Figure 1a), which is a constant-time variant of the previously published 2D [^{15}N,^{1}H]-zero-quantum-TROSY (Pervushin et al., 1999). In the following description the density matrix evolution is represented in terms of the product operators, I and S, representing, respectively, the ^{1}H and ^{15}N spins. The relevant magnetization transfer pathways are given by Equation 10:

$$I_z \rightarrow ZQ_- \exp[-2R^{ZQ}T + i2\Omega^{ZQ}t_1] \rightarrow I^- \quad (10a)$$

$$I_z \rightarrow DQ_+ \exp[-2R^{DQ}T - i2\Omega^{DQ}t_1] \rightarrow I^- \quad (10b)$$

2T is the duration of the constant-time period, $\Omega^{ZQ} = \Omega_I - \Omega_S$, $\Omega^{DQ} = \Omega_I + \Omega_S$, Ω_I and Ω_S are the chemical shifts relative to the carrier frequency of the spins I and S, R^{ZQ} and R^{DQ} are the relaxation rates of the zero- and double-quantum coherences (see Theory). The natural logarithm of the ratio of the signal intensities in the corresponding double quantum, A^{DQ}, and zero-quantum, A^{ZQ}, subspectra provides an estimation of the cross-correlated relaxation rates R_{cc}^{csa} and R_{cc}^{csx}:

$$R_{cc}^{csa} + R_{cc}^{csx} = \ln(A^{DQ}/A^{ZQ})/(4T) \quad (11)$$

2D $^{h1}J_{HN}$,$^{h2}J_{NN}$-quantitative [^{15}N,^{1}H]-TROSY

For studies of $^{h1}J_{HN}$ and $^{h2}J_{NN}$ scalar coupling constants across hydrogen bonds in nucleic acids we introduce the experimental scheme of Figure 1b, which employs the fact that the ZQ and DQ coherences evolve with the difference or sum of the coupling constants J_{IM} and J_{SM} to a remote spin M, respectively. This scheme becomes especially effective for those residues where the CSX interference compensates for the difference in the relaxation rates of the DQ and ZQ coherences due to the CSA/CSA cross-correlated relaxation. In the experimental scheme of Figure 1b performed with the line marked as $^{15}N_d$(I), an additional ^{15}N 180° pulse is employed to selectively invert the remote spin M in such a manner that the magnetization transferred due to the scalar couplings is not refocused, resulting in the interferogram I. A reference interferogram II is acquired with the line marked as $^{15}N_d$(II), where the identical pulse is used to decouple the spin M. The interferograms I and II are separately processed and ZQ and DQ subspectra are extracted from each of the two interferograms. The difference and the sum of the coupling constants is then calculated from the ratio of the signal amplitudes, A^I and A^{II}, in the experiments I and II for the ZQ and DQ subspectra according to Equation 12:

$$A^I/A^{II}(ZQ) = \cos[\pi(^{h1}J_{HN} - {}^{h2}J_{NN})(2T - pw)]/\cos[\pi(^{h1}J_{HN} - {}^{h2}J_{NN})pw] \quad (12a)$$

$$A^I/A^{II}(DQ) = \cos[\pi(^{h1}J_{HN} + {}^{h2}J_{NN})(2T - pw)]/\cos[\pi(^{h1}J_{HN} + {}^{h2}J_{NN})pw] \quad (12b)$$

where 2T is the constant time period and pw is the pulse length of the pulses ψ_2 and ζ_1. To eliminate a necessity for the back-prediction of a few initial points in t_1 caused by the finite length of the pulse ζ_1, the

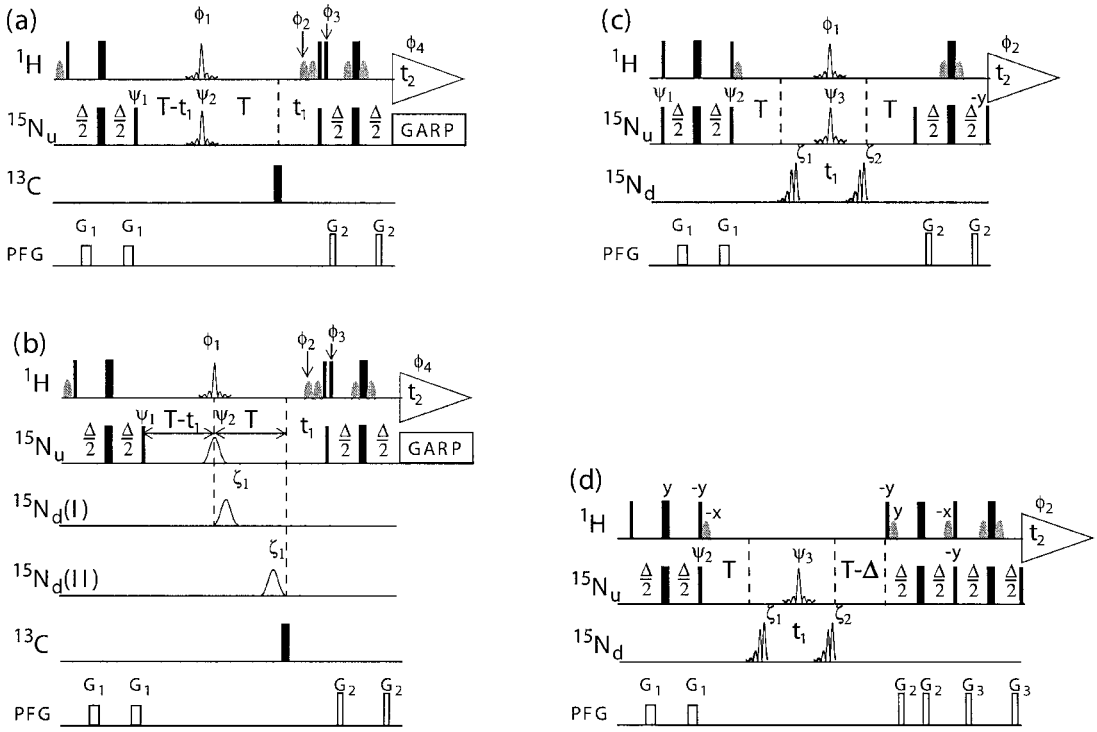

Figure 1. (a) The basic 2D [^{15}N,^{1}H]-zero- and double-quantum TROSY experiment used to detect and suppress conformational exchange induced transverse relaxation in nucleic acids. (b), The 2D $^{h1}J_{HN}$,$^{h2}J_{NN}$-quantitative [^{15}N,^{1}H]-ZQ,DQ-TROSY experiment to measure $^{h1}J_{HN}$ and $^{h2}J_{NN}$ scalar coupling constants across hydrogen bonds in nucleic acids. (c) 2D ($^{h2}J_{NN}$ +$^{h1}J_{NH}$)-correlation-[^{15}N,^{1}H]-TROSY experiment to correlate $^{1}H^{N}$ chemical shifts of bases with the chemical shifts of the tertiary ^{15}N spins across hydrogen bonds in nucleic acids. (d) The 2D $^{h2}J_{NN}$-correlation-[^{15}N,^{1}H]-single-quantum TROSY experiment to detect chemical shifts of the tertiary nitrogen-15 across hydrogen bonds. In the experimental schemes, narrow and wide bars indicate non-selective 90° and 180° pulses applied at the ^{1}H, the '^{15}N-upfield' ($^{15}N_u$) and ^{13}C frequencies, with the carrier offsets placed at 12 ppm, 153 ppm and 145 ppm, respectively. In the experimental schemes (a), (c) and (d) the '^{15}N downfield' ($^{15}N_d$) frequency of 209 ppm is used for the band-selective shaped ^{15}N pulses represented by curved shapes on the line marked $^{15}N_d$. Water saturation is minimized by keeping the water magnetization along the +z-axis during the entire experiment, which is achieved by the application of the off-resonance water-selective 90° rf-pulses indicated by shaded shapes on the line ^{1}H (Piotto et al., 1992). The corresponding constant time delays are compensated for these pulses. The delay for the magnetization transfer is $\Delta = 5.4$ ms. The line marked PFG indicates the pulsed magnetic field gradients applied along the z-axis. The gradients are: G_1, amplitude 20 G/cm, duration 2 ms; $G_2$and G_3, 32 G/cm, 1 ms. In the experimental scheme (a) the constant time delay $2\boldsymbol{T} = 55$ ms, the phases for the rf-pulses are: $\phi_1 = \{x\}$; $\phi_2 = \{x\}$; $\phi_3 = \{x\}$; $\phi_4 = \{x, -x\}$; $\psi_1 = \{x\}$; $\psi_2 = \{x\}$; x on all pulses without phase specification. ϕ_1 and ψ_2 are the refocusing ($M_y \rightarrow -M_y$) RE-BURP pulses (Geen and Freeman, 1991), with a duration of 1.4 ms and 1.2 ms and $\gamma B_1(\max) = 4.4$ kHz and 5.133 kHz, respectively. The complex interferogram I is obtained by recording a second FID for each t_1 delay with ϕ_2 and ϕ_3 inverted. In the same way the complex interferogram II is measured in the interleaved manner by resetting the phase $\psi_1 = \{-y\}$. The addition or subtraction of the complex interferograms I and II followed by the transformation as described by Kay et al. (1992) results in phase-sensitive 2D zero- or double-quantum [^{1}H,^{15}N]-correlation spectra, respectively. In the experimental scheme (b) two sets of zero- and double-quantum spectra are collected. The set I is obtained using the '^{15}N downfield' pulse scheme marked with $^{15}N_d$(I), where the evolution due to the scalar coupling across the hydrogen bond is not refocused. The set II is measured using the $^{15}N_d$(II) scheme, where this evolution is refocused. The coupling constants are estimated from the data sets as described in the text. The constant time delay $2\boldsymbol{T} = 50$ ms. The phase $\zeta_1 = \{x\}$, the pulses ζ_1 and ψ_2 are the 180° gaussian-shaped pulses with a duration of 1 ms and $\gamma B_1(\max) = 1$ kHz. The phases of the other rf-pulses and the transformation protocol are the same as for scheme (a). To achieve higher precision of the coupling constant measurements the experimental scheme of (b) is performed separately for the A=T and G≡C pairs, with the $^{15}N_u$ and $^{15}N_d$ offsets placed at 159.5 ppm and 222.5 ppm, respectively, for the A=T pairs and at 147.5 ppm and 195.5 ppm, respectively, for the G≡C pairs. In the experimental scheme (c) the constant time delay $2\boldsymbol{T} = 38.5$ ms. The phases for the rf-pulses are: $\phi_1 = \{x\}$; $\phi_2 = \{x, -x, -y, y, -x, x, y, -y, -x, x, y, -y, x, -x, -y, y\}$; $\psi_1 = \{-x, x, -y, y\}$; $\psi_2 = \{y, -y, x, -x\}$; $\psi_3 = \{x\}$; $\zeta_1 = \{4x, 4(-x)\}$; $\zeta_2 = \{8x, 8(-x)\}$; x on all pulses without phase specification. ϕ_1 and ψ_3 are the refocusing ($M_y \rightarrow -M_y$) RE-BURP pulses (Geen and Freeman, 1991), with a duration of 1.4 ms and 1.2 ms and $\gamma B_1(\max) = 4.4$ kHz and 5.133 kHz, respectively. ζ_1 and ζ_2 are the excitation (M_z M_x) E-BURP-2 pulses (Geen and Freeman, 1991), with a duration of 0.8 ms and $\gamma B_1(\max) = 5$ kHz. The States-TPPI quadrature detection (Marion et al., 1989) is implemented with the pulse ζ_2. The experimental setup of the scheme (d) is identical to scheme (c) with the exception of the constant time delay $2\boldsymbol{T} = 55$ ms and the phases $\psi_2 = \{y, -y, -x, x\}$ and $\phi_2 = \{y, -y, -x, x, -y, y, x, -x, -y, y, x, -x, y, -y, -x, x\}$. In (a)–(c), the evolution due to the intra-base homonuclear scalar couplings J_{H3H5} and J_{H3H6} in thymine and J_{H1H2} in guanine during the long time period 2T is refocused by the application of the $^{1}H^{N}$ selective RE-BURP ϕ_1 pulse (Pervushin et al., 2000).

pulses ζ_1 are shifted by the time pw/2 relative to the time-points indicated by dashed lines in Figure 1b. The off-resonance application of the pulses ζ_1 requires a slight zero-order phase correction in the ω_1 dimension. The standard deviations of the resulting scalar coupling values are calculated by the error propagation method, where the rmsd of the noise in the spectrum was used as the uncertainty of the experimental peak amplitude.

2D ($^{h2}J_{NN}$ + $^{h1}J_{NH}$)-correlation-[^{15}N,^{1}H]-TROSY

The proposed experimental scheme of Figure 1c employs the DQ coherence to transfer magnetization across hydrogen bonds using the sum of the two coupling constants $^{h1}J_{HN}$ + $^{h2}J_{NN}$ to correlate the ^{1}H^{N} chemical shifts of bases with the chemical shifts of the tertiary ^{15}N spins across hydrogen bonds in nucleic acids. The experiment is effective for the residues where transverse relaxation of the ^{1}H and ^{15}N spins is dominated by conformational exchange, which can be effectively suppressed by the CSX interference. Since the CSX interaction is expected to be the dominant source of relaxation only for a few residues, the 2D ($^{h1}J_{HN}$ + $^{h2}J_{NN}$)-correlation-[^{15}N,^{1}H]-TROSY can be complemented by the conventional TROSY scheme where the single-quantum TROSY component of the ^{15}N doublet is used to transfer magnetization across hydrogen bonds utilizing only the $^{h2}J_{NN}$ coupling. The corresponding experimental scheme is shown in Figure 1d.

Results and discussion

The experimental schemes which are newly introduced in this paper (Figure 1) are derived from the basic 2D zero-quantum-[^{15}N,^{1}H]-TROSY experiment (Pervushin et al., 1999). In contrast to the 2D ZQ-[^{15}N,^{1}H]-TROSY, the experimental scheme of Figure 1a recovers both ZQ and DQ magnetization transfer pathways (see Equations 1 and 2 in Pervushin et al. (1999)) and records corresponding ZQ and DQ chemical shifts in the constant-time manner. By introducing GARP broadband decoupling during signal acquisition both ZQ and DQ pathways are detected via the same in-phase proton spin operator I^-, enabling the direct comparison of the signal intensities in the corresponding ZQ and DQ 2D [^{15}N,^{1}H]-correlation spectra. The basic experimental scheme of Figure 1a was applied to the partially ^{15}N,^{13}C labeled 14-mer DNA duplex representing a BS2 operator and to the uniformly ^{15}N,^{13}C labeled BS2 DNA duplex in the 17 kDa complex with the *Antp* homeodomain.

Table 1. Values and standard deviations of the CSA and CSX cross-correlated relaxation rates of the partially ^{15}N,^{13}C-labeled 14-mer DNA duplex free in solution measured with 2D [^{15}N,^{1}H]-ZQ,DQ-TROSY

Residue	$R_{cc}^{csa} + R_{cc}^{csx}$ [a] (s^{-1})	
	T = 30 °C	T = 37 °C
G^5	7.0 ± 0.2[b]	5.36 ± 0.7
G^{12}	7.3 ± 0.2	6.40 ± 0.7
$T^{21(a)}$	1.1 ± 0.3	−3.74 ± 0.8[c]
$T^{21(b)}$	−1.2 ± 0.2	−3.74 ± 0.8[c]

[a]The sum of the CSA and CSX cross-correlated relaxation rates $R_{cc}^{csa} + R_{cc}^{csx}$ is obtained from the relaxation rates of the ZQ and DQ coherences (see Theory).
[b]The standard deviations were obtained by the error propagation method using the rmsd of the spectral noise as the uncertainty of the peak amplitude measurement.
[c]At 37 °C signals $T^{21(a)}$ and $T^{21(b)}$ collapse.

Figures 2a and b compare the ZQ- and DQ-[^{15}N,^{1}H]-TROSY subspectra of the free DNA duplex at 30 °C. The partial labeling of the selected nucleotides indicated on the schematic drawings of the DNA duplex (Figure 2, top) allowed observation of apparent doubling of the [^{15}N,^{1}H]-correlation cross peak of T^{21}. The two cross peaks assigned to T^{21} might represent two distinct conformational states with relative populations of 0.3 and 0.7, as is derived from the relative peak intensities. The increase of the exchange rate at 37 °C results in the collapse of these resonances into a broad peak (Figures 2c and d). At the elevated temperature the presence of conformational exchange-induced transverse relaxation is detected by a comparison of the signal intensities in the ZQ- and DQ-subspectra using the 1D slices along the ω_2 dimension shown on the inserts in Figures 2c and d. The transverse relaxation rates of the corresponding ZQ- and DQ-coherences of T^{21} collected in Table 1 indicate that conformational exchange-induced line broadening is the dominant source of transverse relaxation for the ^{1}H and ^{15}N spins. The suppression of the conformational exchange-induced transverse relaxation in the DQ-[^{15}N,^{1}H]-correlation subspectrum results in the significant increase of the signal intensity of the [^{15}N,^{1}H]-correlation cross peak of T^{21}.

The cross-correlated CSX relaxation rates of the uniformly ^{15}N,^{13}C-labeled DNA duplex in a complex with the *Antp* homeodomain measured at 20 °C are

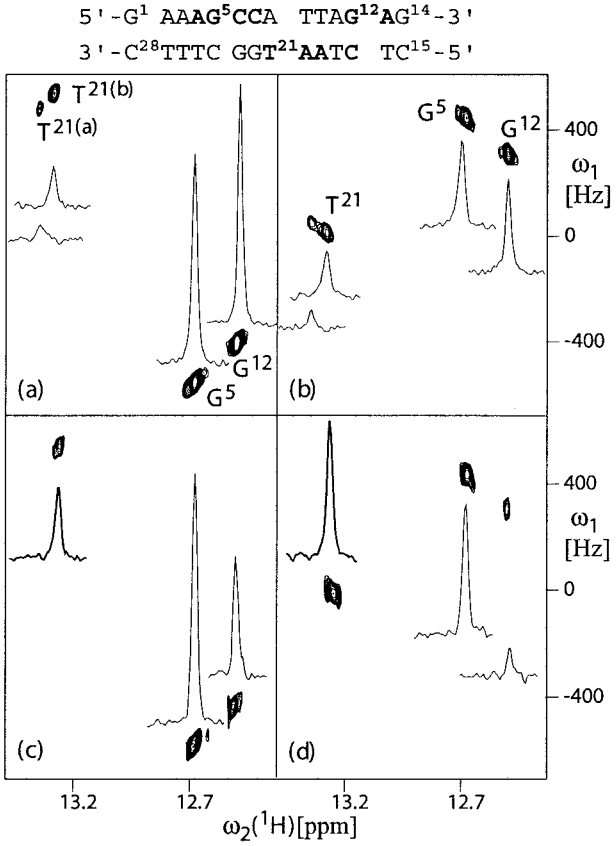

Figure 2. Detection of conformational exchange-induced transverse relaxation in the BS2 DNA duplex. (a) and (c) Contour plots and cross sections along $\omega_2(^1H)$ through the individual cross peaks from [^{15}N,^1H]-zero-quantum TROSY spectra of the partially ^{13}C,^{15}N-labeled DNA duplex (see insert on the top, bold letters identify the nucleotides that contain ^{15}N in the partially labelled duplex) at T = 30 °C and 37 °C, respectively. (b) and (d) Corresponding contour plots from [^{15}N,^1H]-double-quantum TROSY spectra extracted from the same data set. The spectra were recorded with the TROSY experimental scheme of Figure 1a on a Bruker *Avance*-800 spectrometer equipped with a ^1H-{^{13}C,^{15}N} triple-resonance probehead (DNA duplex concentration = 2 mM, solvent 95% H_2O/5% D_2O, pH = 6.0). Forty complex t_1 points were acquired with the 1 s interscan delay and t_{1max} = 8 ms and t_{2max} = 51 ms, resulting in 2.5 h of measuring time. Chemical shifts relative to DSS (in ppm) are indicated in the $\omega_2(^1H)$ dimension and shifts (in Hz) relative to the centre of the spectrum are indicated in the ω_1 dimension.

derived from the signal intensities in the ZQ- and DQ-subspectra shown in Figures 3 a and b. A comparison of the 1D slices along the ω_2 dimension presented in Figure 3c indicates the presence of the conformational exchange localized at the residues T^9, T^{26} and T^{27} (see Table 2). The 2D [^{15}N,^1H]-ZQ- and DQ-TROSY experiments measured at different temperatures between 15 °C and 37 °C revealed no apparent resonance doubling for these residues, which might indicate that the exchange rates remain on the intermediate to fast time scale. To distinguish the relative contributions of the CSA and CSX mechanisms to overall relaxation, the residues T^{10}, T^{18}, T^{25}, T^{21}, G^5, G^{12} and G^{22} were used as references for which no CSX contribution to transverse relaxation was assumed. The choice of those residues was based on the absence of detectable rf-field strength dependence in the ^{15}N $T_{1\rho}$ measurements (Szyperski et al., 1993; data not shown). Since in the DNA duplex only small variation of the ^1H and ^{15}N CSA tensors within residues of the same type can be reasonably assumed (Pervushin et al., 1998a), the average CSA relaxation rates can be calculated and then used to estimate the CSX relaxation contribution (see Table 2).

For the particular case of residue T^{21} in the free DNA duplex and for T^{26} and T^{27} in the DNA complex the large value and the negative sign of the R_{cc}^{csx} term was established. This observation can be used to improve relaxation properties of the double-quantum coherence, which is considered to be relaxationally unfavourable due to the CSA/CSA interference effect (Pervushin et al., 1998a). In turn,

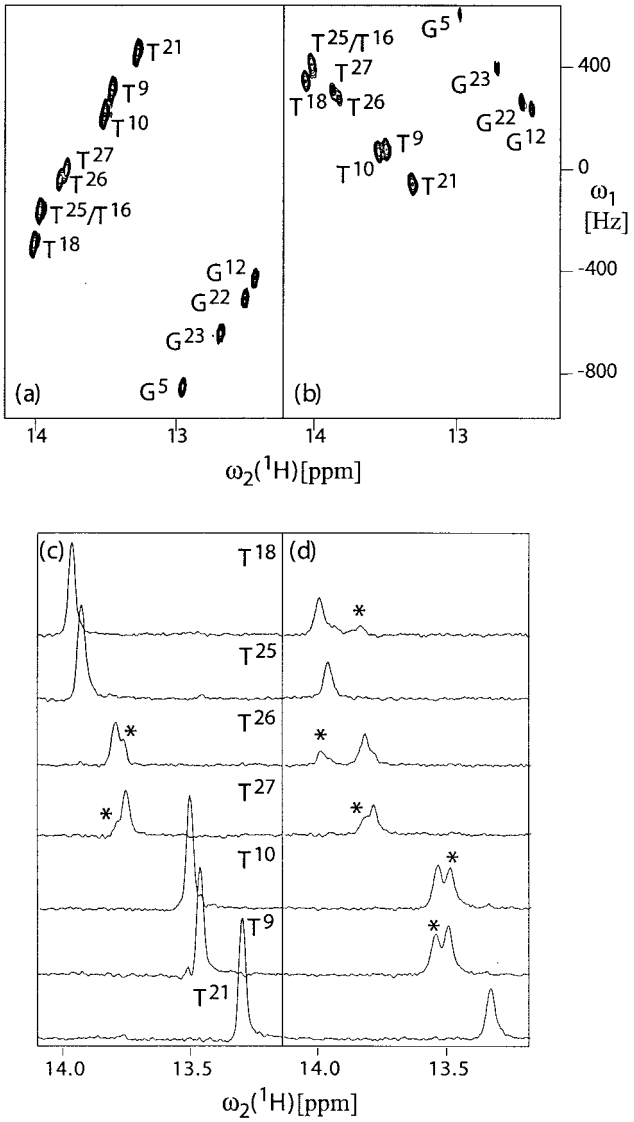

Figure 3. Detection of conformational exchange-induced transverse relaxation in the *Antp* homeodomain-DNA complex. (a) and (b) Contour plots from [^{15}N,^{1}H]-zero-quantum TROSY and [^{15}N,^{1}H]-double-quantum TROSY spectra, respectively, at T = 20 °C. (c) and (d) Cross sections along $\omega_2(^1\mathrm{H})$ through the individual cross peaks taken from the spectra (a) and (b), respectively. The spectra were recorded with the TROSY experimental scheme of Figure 1a on a Bruker *Avance*-800 spectrometer (*Antp* homeodomain–DNA complex concentration = 1 mM, solvent 95% H_2O/5% D_2O, pH = 6.0, T = 20 °C). Forty complex t_1 points were acquired with the 1 s interscan delay and $t_{1\max}$ = 8 ms and $t_{2\max}$ = 51 ms, resulting in 2.5 h of measuring time. An asterisk denotes the leakage of a neighbouring peak. Chemical shifts relative to DSS (in ppm) are indicated in the $\omega_2(^1\mathrm{H})$ dimension and shifts (in Hz) relative to the centre of the spectrum are indicated in the ω_1 dimension.

the use of double-quantum coherence enables to recruit both $^{h2}J_{NN}$ and $^{h1}J_{NH}$ coupling constants to relay magnetization via the sum of coupling constants $^{h2}J_{NN} + {}^{h1}J_{NH}$ across the hydrogen bond to the tertiary ^{15}N position of the second base in the Watson–Crick base pair. The use of the two trans-hydrogen bond couplings enables to reduce the total magnetization transfer time by 30% compared with the arrangement when solely $^{h2}J_{NN}$ coupling is employed. The sensitivity of this 2D ($^{h2}J_{NN} + {}^{h1}J_{NH}$)-correlation-[^{15}N,^{1}H]-TROSY experiment is further enhanced by the use of both ^{1}H and ^{15}N steady state magnetizations (Pervushin et al., 1998c). Even for the most demanding case of the relatively large DNA complex of 17 kDa, 2D ($^{h2}J_{NN} + {}^{h1}J_{NH}$)-correlation-[^{15}N,^{1}H]-TROSY provides an improved sensitivity

Table 2. Values and standard deviations of the CSA and CSX cross-correlated relaxation rates of the uniformly ^{15}N,^{13}C-labeled 14-mer DNA duplex in a complex with the *Antp* homeodomain measured with the 2D [^{15}N,^{1}H]-ZQ,DQ-TROSY at 20 °C

Residue	$R_{cc}^{csa} + R_{cc}^{csx}$ (s^{-1})[a]	R_{cc}^{csx} (s^{-1})[b]
G^5	8.2 ± 1.0[c]	–
G^{12}	7.5 ± 1.0	–
G^{22}	8.0 ± 1.0	–
G^{23}	6.4 ± 1.2	-1.5 ± 2.2
T^9	6.6 ± 0.2	-1.0 ± 0.5
T^{10}	8.0 ± 0.3	–
T^{18}	7.4 ± 0.3	–
T^{21}	7.2 ± 0.2	–
T^{25}	7.9 ± 0.2	–
T^{26}	2.4 ± 0.3	-5.2 ± 0.6
T^{27}	3.7 ± 0.3	-3.9 ± 0.6

[a]The sum of the CSA and CSX cross-correlated relaxation rates $R_{cc}^{csa} + R_{cc}^{csx}$ is obtained from the relaxation rates of the ZQ and DQ coherences (see Theory).

[b]The CSX cross-correlated relaxation rates R_{cc}^{csx} are estimated as the difference between $R_{cc}^{csa} + R_{cc}^{csx}$ and the average relaxation rates of 7.6 ± 0.3 s^{-1} for T (averaged over the residues T^{10}, T^{18}, T^{25} and T^{21}) and 7.9 ± 1.0 s^{-1} for G (averaged over the residues G^5, $G^{12}$and G^{22}), respectively, where no CSX relaxation was observed by $T_{1\rho}$ (^{15}N) CPMG measurements.

[c]The standard deviations were obtained by the error propagation method using the rmsd of the spectral noise as the uncertainty of the peak amplitude measurement.

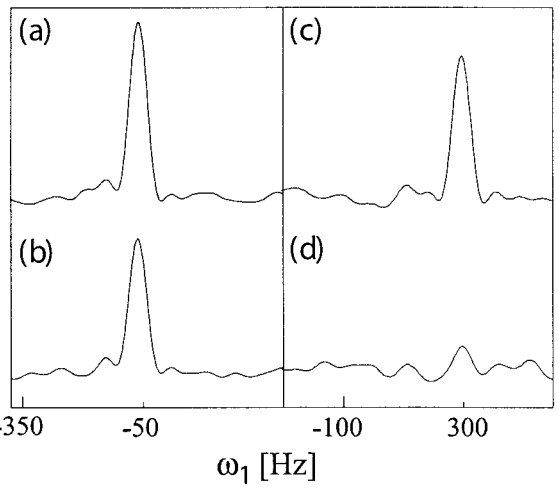

Figure 4. (a) and (c) The 1D slices along $\omega_1(^{15}N)$ taken at the position of the correlation peaks of T^{26} from the reference 2D zero- and double-quantum [^{1}H,^{15}N] correlation spectra extracted from the interferogram II. (b) and (d) The corresponding 1D slices taken from the 2D zero- and double-quantum [^{1}H,^{15}N] correlation spectra extracted from the interferogram I, where a part of the magnetization is transferred across-hydrogen bond. The spectra are recorded using the experimental scheme of Figure 1b with the uniformly ^{15}N,^{13}C-labeled *Antp* homeodomain-DNA complex (*Antp* homeodomain-DNA complex concentration = 1 mM, solvent 95% H_2O/ 5% D_2O, pH = 6.0, T = 20 °C). The signal intensities are used to calculate the $^{h1}J_{HN}$ and $^{h2}J_{NN}$ coupling constants. For each interferogram 34 complex t_1 points were acquired with the 1 s interscan delay and t_{1max} = 6.4 ms and t_{2max} = 51 ms resulting in 14 h of total measuring time. Chemical shifts (in Hz) relative to the centre of the spectrum are indicated in the $\omega_1(^{15}N)$ dimension.

for the residues affected by the conformational exchange when compared to the 2D single-quantum $^{h2}J_{NN}$-correlation-[^{15}N,^{1}H]-TROSY (Figure 5).

The constructive use of the CSX interference might result in comparable relaxation properties of the ZQ- and DQ-coherences, as is the case for the residues T^{26} and T^{27} (Figure 3c). Since the evolution of the ZQ- and DQ-coherences proceeds under the difference and the sum of the $^{h2}J_{NN}$ and $^{h1}J_{NH}$ coupling constants, it is possible to derive values of each individual coupling constant by comparison of the corresponding signal intensities in the ZQ- and DQ-subspectra measured when the evolution due to coupling across hydrogen bonds is refocused or not (see Figure 4). The obtained individual coupling constants are summarized in Table 3.

The efficiency of the suppression of the transverse relaxation induced by conformational exchange on the intermediate to fast time scale depends primarily on the relative differences in the chemical shifts between exchanging conformers. Complete suppression can be achieved for the case of two-site exchange when $\Delta\delta\omega_H^{12} = \Delta\delta\omega_N^{12}$. Note that the degree of suppression is affected neither by the rate of exchange nor by the relative population of the exchanging conformers, as is implied by Equations 6. However, the theoretical analysis indicates rapid deterioration of the suppression of CSX relaxation as the number of exchanging conformers increases.

Overall, the analysis of double- and zero-quantum relaxation rates of the base ^{1}H-^{15}N moieties showed that for certain residues the contribution of conformational exchange-induced transverse relaxation might represent a dominant relaxation mechanism, which can be effectively suppressed by spectroscopic means. We believe that a variety of NMR experiments currently employed for resonance assignment and collection of structural constraints can benefit from the

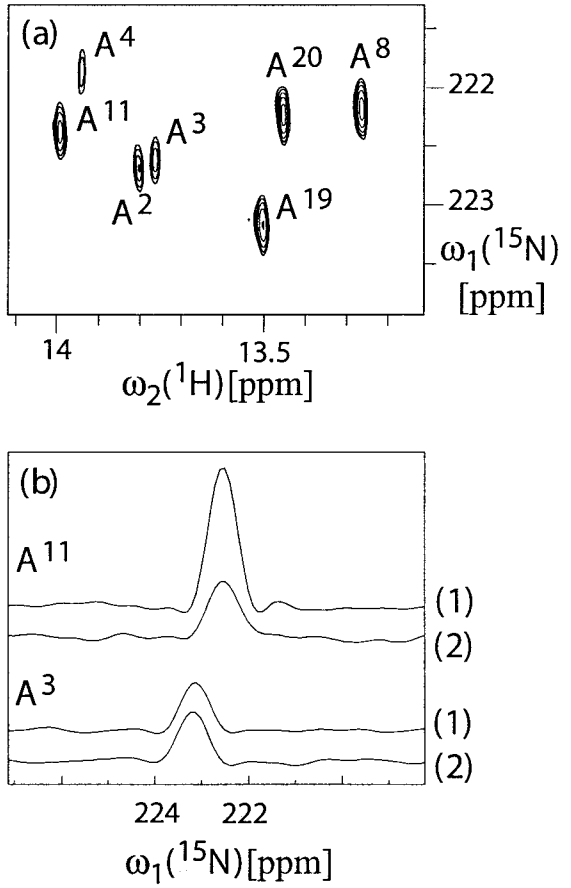

Figure 5. (a) Contour plot from the 2D ($^{h2}J_{NN} + {}^{h1}J_{NH}$)-correlation-[^{15}N,^{1}H]-TROSY spectrum, showing the relayed [$^{15}N_1$(A),$^{1}H_3$(T)] cross peaks of the A=T base pairs measured with the experimental scheme of Figure 1c. (b) The 1D slices along $\omega_1(^{15}N)$ taken at the position of the correlation peaks of [$^{15}N_1$(A11),$^{1}H_3$(T18)] and [$^{15}N_1$(A3),$^{1}H_3$(T26)] in spectrum (a) (lower trace in the pairs of slices) and in the 2D single-quantum $^{h2}J_{NN}$-correlation-[^{15}N,^{1}H]-TROSY spectrum measured with the experimental scheme of Figure 1d (upper trace in the pairs of slices). For each spectrum 64 complex t_1 points were acquired with the 1 s interscan delay and $t_{1max} = 15$ ms and $t_{2max} = 51$ ms, resulting in 4 h of measuring time. Chemical shifts relative to DSS (in ppm) are indicated in both dimensions.

rational optimization of relaxation properties, which constitutes the essence of the TROSY approach.

Acknowledgements

We thank Prof. Kurt Wüthrich, ETH Zürich, and Prof. Masatsune Kainosho, Tokyo Metropolitan University, for making the samples of the BS2 DNA and the *Antp* homeodomain-DNA complex available for the studies and for helpful discussion.

Table 3. Values and standard deviations of the ^{1}H-^{15}N and ^{15}N-^{15}N scalar spin–spin couplings across hydrogen bonds, $^{h1}J_{NH}$ and $^{h2}J_{NN}$, in Watson–Crick base pairs of the 14-mer DNA duplex in a complex with the *Antp* homeodomain at 20 °C measured with the 2D $^{h1}J_{HN}$,$^{h2}J_{NN}$-quantitative [^{15}N,^{1}H]-ZQ,DQ-TROSY.

Residue	$^{h2}J_{NN}$ (Hz)[a]	$^{h1}J_{NH}$ (Hz)[a]
G^5	6.6 ± 0.4[b]	3.0 ± 0.4
G^{12}	6.4 ± 0.4	2.9 ± 0.4
G^{22}	6.6 ± 0.4	3.1 ± 0.4
G^{23}	6.3 ± 0.4	3.4 ± 0.4
T^9	6.6 ± 0.3	1.8 ± 0.3
T^{10}	7.2 ± 0.3	2.1 ± 0.3
T^{18}	7.0 ± 0.3	2.4 ± 0.3
T^{21}	6.8 ± 0.3	2.2 ± 0.3
T^{25}	6.8 ± 0.3	2.3 ± 0.3
T^{26}	6.5 ± 0.6	2.3 ± 0.6
T^{27}	6.5 ± 0.8	2.6 ± 0.8

[a]The values of coupling constants were calculated from the sum and the difference of the corresponding couplings obtained by the numerical solution of Equations 12.
[b]The standard deviations were obtained by the error propagation method using the rmsd of the spectral noise as the uncertainty of the peak amplitude measurement.

References

Abragam, A. (1961) *The Principles of Nuclear Magnetism*, Clarendon, Oxford.
Boisbouvier, J., Gans, P., Blackledge, M., Brutscher, B. and Marion, D. (1999) *J. Am. Chem. Soc.*, **121**, 7700–7701.
Brutscher, B., Boisbouvier, J., Pardi, A., Marion, D. and Simorre, J.P. (1998) *J. Am. Chem. Soc.*, **120**, 11845–11851.
Choe, B., Cook, G.W. and Krishna, N.R. (1991) *J. Magn. Reson.*, **94**, 387–393.
Deverell, C., Morgan, R.E. and Strange, J.H. (1970) *Mol. Phys.*, **18**, 553–559.
Farrow, N.A., Zhang, O.W., Forman-Kay, J.D. and Kay, L.E. (1994) *J. Biomol. NMR*, **4**, 727–734.
Feigon, J., Denny, W.A., Leupin, W. and Kearns, D.R. (1983) *Biochemistry*, **22**, 5930–5942.
Feigon, J., Wang, A.H.J., Van der Marel, G.A., Van Boom, J.H. and Rich, A. (1984) *Nucleic Acids Res.*, **12**, 1243–1263.
Fernandez, C., Szyperski, T., Ono, A., Iwai, H., Tate, S., Kainosho, M. and Wüthrich, K. (1998) *J. Biomol. NMR*, **12**, 25–37.
Geen, H. and Freeman, R. (1991) *J. Magn. Reson.*, **93**, 93–141.
Goldman, M. (1984) *J. Magn. Reson.*, **60**, 437–452.
Kaplan, J.I. and Fraenkel, G. (1980) *NMR of Chemically Exchanging Systems*, Academic Press, San Diego, CA.
Kay, L.E., Keifer, P. and Saarinen, T. (1992) *J. Am. Chem. Soc.*, **114**, 10663–10665.
Kloiber, K. and Konrat, R. (2000) *J. Biomol. NMR*, **18**, 33–42.
Kumar, P. and Kumar, A. (1996) *J. Magn. Reson.*, **A119**, 29–37.

Madhu, P.K., Grandori, R., Mandal, P.K., Hohenthanner, K. and Müller, N. (2001) *J. Biomol. NMR*, **20**, 31–37.
Marion, D., Ikura, M., Tschudin, R. and Bax, A. (1989) *J. Magn. Reson.*, **85**, 393–399.
Meissner, A. and Sørensen, O.W. (1999) *J. Magn. Reson.*, **139**, 447–450.
Mok, Y.K., Kay, C.M., Kay, L.E. and Forman-Kay, J. (1999) *J. Mol. Biol.*, **289**, 619–638.
Moseley, H.N.B., Lee, W., Arrowsmith, C.H. and Krishna, N.R. (1997) *Biochemistry*, **36**, 5293–5299.
Muller, M., Affolter, M., Leupin, W., Otting, G., Wüthrich, K. and Gehring, W.J. (1988) *EMBO J.*, **7**, 4299–4304.
Neri, D., Billeter, M., Wider, G. and Wüthrich, K. (1992) *Science*, **257**, 1559–1563.
Nicholson, L.K., Yamazaki, T., Torchia, D.A., Grzesiek, S., Bax, A., Stahl, S.J., Kaufman, J.D., Wingfield, P.T., Lam, P.Y.S., Jadhav, P.K., Hodge, C.N., Domaille, P.J. and Chang, C.H. (1995) *Nat. Struct. Biol.*, **2**, 274–280.
Pervushin, K., Fernandez, C., Riek, R., Ono, A., Kainosho, M. and Wüthrich, K. (2000) *J. Biomol. NMR*, **16**, 39–46.
Pervushin, K., Ono, A., Fernandez, C., Szyperski, T., Kainosho, M. and Wüthrich, K. (1998a) *Proc. Natl. Acad. Sci. USA*, **95**, 14147–14151.
Pervushin, K., Riek, R., Wider, G. and Wüthrich, K. (1997) *Proc. Natl. Acad. Sci. USA*, **94**, 12366–12371.
Pervushin, K., Riek, R., Wider, G. and Wüthrich, K. (1998b) *J. Am. Chem. Soc.*, **120**, 6394–6400.
Pervushin, K., Wider, G., Riek, R. and Wüthrich, K. (1999) *Proc. Natl. Acad. Sci. USA*, **96**, 9607–9612.
Pervushin, K., Wider, G. and Wüthrich, K. (1998c) *J. Biomol. NMR*, **12**, 345–348.
Piotto, M., Saudek, V. and Sklenar, V. (1992) *J. Biomol. NMR*, **2**, 661–665.
Rance, M. (1988) *J. Am. Chem. Soc.*, **110**, 1973–1974.
Riek, R., Pervushin, K., Fernandez, C., Kainosho, M. and Wüthrich, K. (2001) *J. Am. Chem. Soc.*, **123**, 658–664.
Sandstrom, J. (1982) *Dynamic NMR Spectroscopy*, Academic Press, San Diego, CA.
Shimizy, H. (1964) *J. Phys. Chem.*, **40**, 3357–3364.
Skrynnikov, N.R. and Ernst, R.R. (1999) *J. Magn. Reson.*, **137**, 276–280.
Szyperski, T., Luginbuhl, P., Otting, G., Güntert, P. and Wüthrich, K. (1993) *J. Biomol. NMR*, **3**, 151–164.
Tessari, M. and Vuister, G.W. (2000) *J. Biomol. NMR*, **16**, 171–174.
Tropp, J. (1980) *J. Chem. Phys.*, **72**, 6035–6043.
Wider, G. and Wüthrich, K. (1999) *Curr. Opin. Struct. Biol.*, **9**, 594–601.
Yang, D.W. and Kay, L.E. (1999) *J. Am. Chem. Soc.*, **121**, 2571–2575.